The Use of Vibration Data for Liquid Rocket Health Monitoring [1]

Paulo Lozano [2]

Nhut Ho [3]

Manuel Martinez-Sanchez [2]

Rami Mangoubi [4]

Abstract

An approach is presented to the construction of a liquid rocket Health Monitoring (HM) system capable of using both, vibratory and thermodynamic data. Preliminary results are obtained in the area of vibration data tracking/identification, using as a test bed a low-order linear dynamic model of the Space Shuttle Main Engine (SSME) High Pressure Fuel Turbopump (HPFTP). Limitations and future extensions are discussed.

1. Introduction

Liquid propellant rocket engines operate at extremely high power loadings, making component failures both, more likely than in other machinery, and very costly in their consequences. Because of this, substantial efforts have been made to extract as much information as possible from the limited suite of instruments providing data during firings. The objectives are (a) to accurately assess the health status of an engine, (b) to diagnose by post-event data analysis the cause of an anomaly, and/or (c) to provide real-time feedback to engine controllers.

Several approaches have been tested using the Space Shuttle Main Engine (SSME) as a test bed. These include statistical approaches based on engine test history [1], analytic redundancy [2], neural networks[3] and model-based techniques [4, 5].

In all cases, the data and models have been related to what could be called the engine thermodynamic state (pressures, flows, temperatures, shaft speeds), with heavily damped dynamics. Thus, except for possible applications during rapid commanded transients, these methods manipulate essentially steady-state engine variables. The engines, however, have rich lightly damped, vibratory spectra, including both, rotordynamic and case modes. Accelerometer or strain gauge data on these vibrations are routinely used in a "red-line" mode only, although occasional model comparisons are performed off-line during anomaly investigations.

Techniques for modal identification of lightly damped structures are well developed, led by spacecraft applications [6]. By itself, one of these methods (used in conjunction with an array of advanced microsensors) could provide valuable engine health information, giving, for example, advance warning of incipient rubs, bearing degradation or inducer cavitation. Further, fluid-derived inputs to the vibration dynamics are clearly influenced by the thermodynamic state and the power and speed levels of the engine, so that joint use of both, vibratory and thermodynamic monitoring algorithms is desirable.

One difficulty in the path of this unified Health Monitoring (HM) system is the large difference in time scales of the thermodynamic vs. the vibratory data. The former

[2] Department of Aeronautics and Astronautics, Massachusetts Institute of Technology, Cambridge, MA.

[3] Department of Mechanical Engineering, M.I.T. and Control and Dynamical Systems Division, C.S. Draper Laboratory, Cambridge.

[4] Control and Dynamical Systems Division, C.S. Draper Laboratory, Cambridge.

can be sampled, as in the SSME data system, at 50 Hz, which, as shown in [5], is sufficient for discriminating model-based diagnostics. The latter would require on the order of a few kHz, since the basic SSME modes are in the range of 200-1000 Hz; this information is normally stored in analog form for post-test analysis.

In order to combine these two sources of information, a separate layer of processing is required to generate relevant "slowly varying" vibratory information which can then be co-processed together with the thermodynamic data. The general structure of a HM system based on this notion is shown in Fig. 1. For successful implementation, the vibration tracking and identification algorithm should be both computationally economical and robust to the noisy and complex environment of a rocket engine. The Vibration and Rotordynamic Model running concurrently (with inputs from the Thermodynamic Model) has as its purpose to provide additional information to help the final filtering stage refine its estimates and generate accurate diagnoses. All data and model results would, of course, feed into this filter synchronously, at the lower rate (say, 50 Hz.)
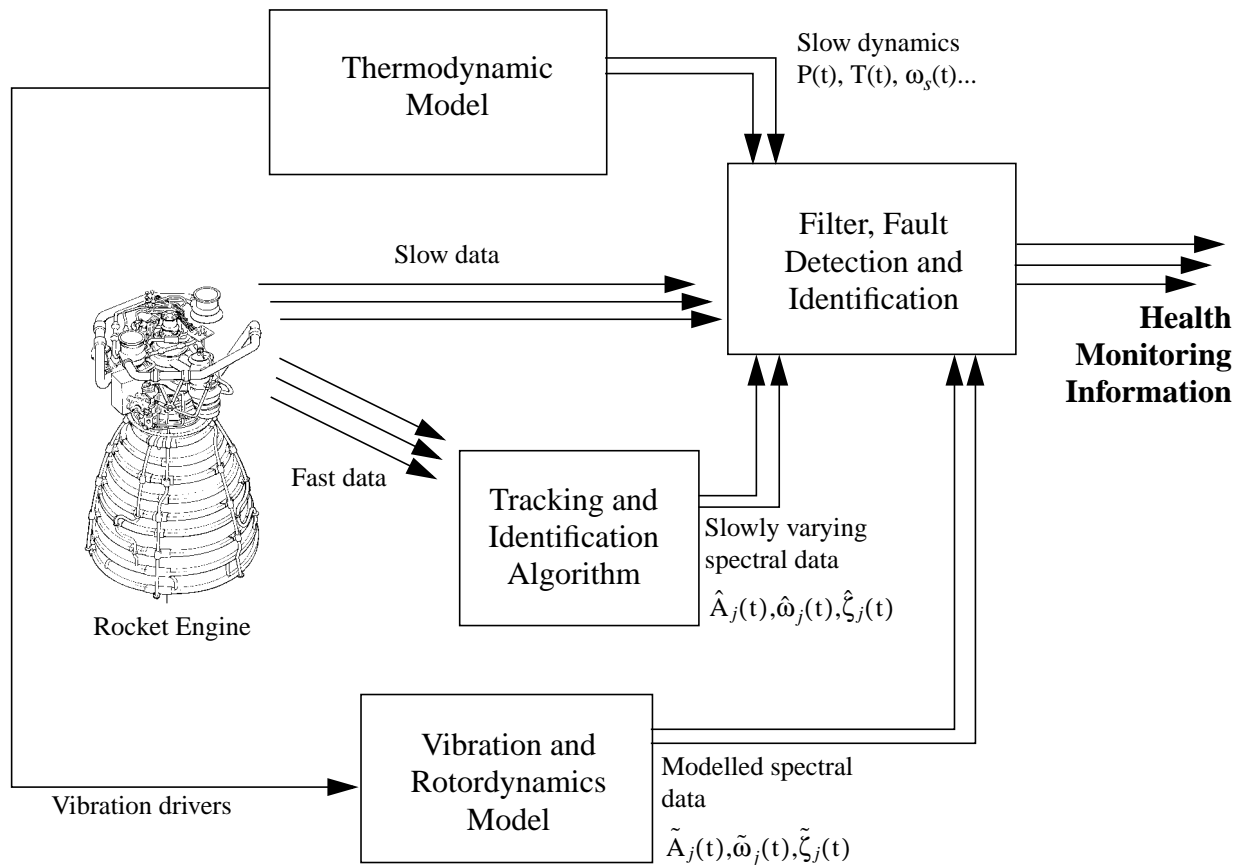

Figure 1. Conceptual unified HM system

This is clearly an ambitious global program. In this paper we restrict our attention to initial versions of the vibration and rotordynamic model and the vibration tracking and identification algorithm (for which, incidentally, the model can serve as a test bed during development.) Left for future work is the synthesis (filtering) stage, as well as many necessary improvements in the vibration signal processing, which will be pointed out in the context of several examples of application of one state-of-the-art algorithm.

This analysis is expected to lead to eventual integration with our related work on thermodynamic modeling [5] into a comprehensive health monitoring system that could be applied to any RLV (Reusable Launch Vehicle) rocket engine.

2. Rotordynamic Model for the HPFTP

The High Pressure Fuel Turbopump (HPFTP) rotor consists of a complex assembly of different parts as shown in Fig. 2.
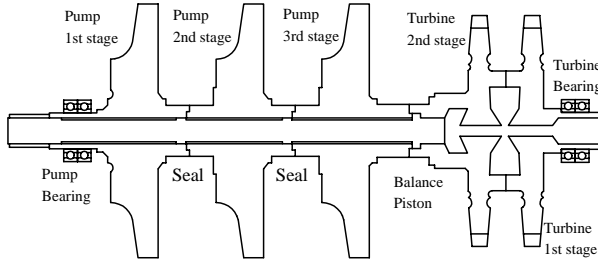

Figure 2. HPFTP rotor - adapted from [7]

There are three centrifugal pump stages mounted on a single beam. One extreme of the beam is held by a bearing (pump bearing) which is attached to the rotor casing, the other extreme is fastened to the turbine's second and first stages. A second bearing (turbine bearing) is mounted at the end of the turbine's first stage. Modeling of a system such as this is done in different ways depending on the accuracy required for the physical representation in a particular application. Our model's main purpose here is to serve as a testbed for the tracking/ identification algorithms, we therefore can relax the precision requirements of more complicated finite element and nonlinear calculations [7, 8, 9].
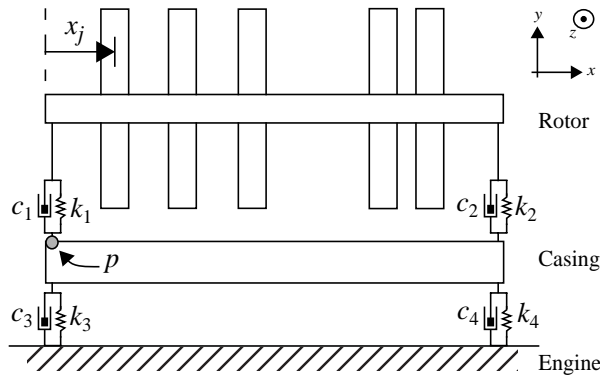

Figure 3. Simplified model of the HPFTP. Point p represents the location of an hypothetical accelerometer used in this study.

We have chosen to perform the derivation of the equations of motion using the Lagrangian formalism which has the advantage of presenting, in a very clear form, the physical interactions involved in the system's dynamics. In our simplified lumped version, the pumps and turbines are considered as solid thin discs mounted over a single symmetric beam with a certain density per unit length (ρ_b), geometrical moment of inertia (I), modulus of elasticity (E) and length (L) as shown in Fig. 3. The disc positions over the shaft (x_j), masses (m_j) and transversal moments of inertia (J_j) were extracted from [7].

The bearings are substituted by elastic springs (with constants k_1 and k_2) and damping devices (c_1 and c_2) which are attached to a heavy bar of density per unit length (ρ_c) and moment of inertia (J_c). This bar is considered as a rough representation of the turbopump casing. Finally, the casing itself is attached to the engine via springs and dampers (k_3, k_4, c_3 and c_4), in our case the engine is considered as ground, completely fixed.

To determine the dynamic behavior, we have to define the allowed degrees of freedom. As shown in Fig. 4, only five will be considered: one for the amplitude of the first bending mode of the rotor beam (f) plus four for each of the displacements e_1, e_2, e_3 and e_4. The bar representing the casing will be considered rigid enough to preclude it from bending.
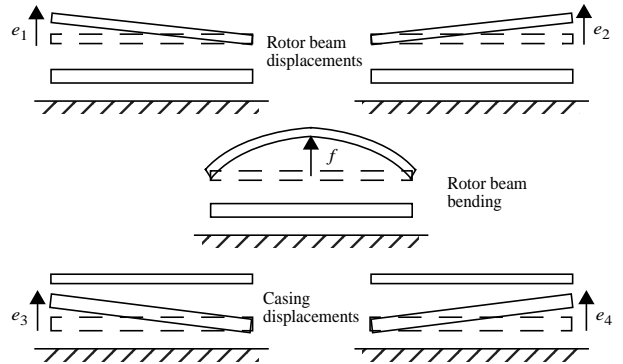

Figure 4. Degrees of freedom

We can take advantage of the intrinsic axial symmetry of this problem to upgrade our model from its one dimensional formulation to a two dimensional one by allowing the degrees of freedom to be complex quantities:

$$q_j = q_{jy} + i q_{jz}$$
$$q_j \equiv \{f, e_1, e_2, e_3, e_4\} \tag{1}$$

We can write the kinetic and potential energies of the system in terms of this set of displacements. The potential energy (V) is a combination of the elastic energy stored in the beam as it bends and the energy stored in each one of the springs:

$$V = \frac{EI\pi^4}{4L^3}f^2 + \frac{1}{2}[k_1(e_1 - e_3)^2 + k_2(e_2 - e_4)^2 + \dots$$
$$\dots + k_3 e_3^2 + k_4 e_4^2 + ik_{yz}y_{yz}^2] \tag{2}$$

The last term in (2) involves the introduction of a cross-coupled interaction of the movements along perpendicular directions: y_{yz} denotes the instantaneous eccentricity of the rotor from its nominal position as a function of the model's five degrees of freedom. These forces typically appear in turbines due to uneven work extraction caused, for example, by variations in the distance between the turbine's blade tips and the casing [10]. k_{yz} is the cross-coupled stiffness coefficient which is found to be a linear function of the torque Γ generated by the turbine and a constant β known as the Alford coefficient:

$$k_{yz} = \frac{\beta\Gamma}{2RH} \tag{3}$$

where R is the mean radius and H the blade height.

The kinetic energy (T) adds up contributions from the movements of the rotor beam (*i*), each one of the discs (*ii*) and the casing (*iii*), plus the inertias of the rotor beam (*iv*), the discs (*v*) and the casing beam (*vi*) about the z axis:

$$T_i = \frac{1}{2}\int_0^L \rho_b\left(\frac{dy_b}{dt}\right)^2 dx \qquad T_{ii} = \frac{1}{2}\sum_{j=1}^5 m_j\left(\frac{dy_b}{dt}\bigg|_{x_j}\right)^2$$

$$T_{iii} = \frac{1}{2}\int_0^L \rho_c\left(\frac{dy_c}{dt}\right)^2 dx \qquad T_{iv} = \frac{1}{2}J_b\left[\frac{d}{dt}\left(\frac{\partial y_b}{\partial x}\right)\right]^2 \tag{4}$$

$$T_v = \frac{1}{2}\sum_{j=1}^5 J_j\left[\frac{d}{dt}\left(\frac{\partial y_b}{\partial x}\bigg|_{x_j}\right)\right]^2 \qquad T_{vi} = \frac{1}{2}J_c\left[\frac{d}{dt}\left(\frac{\partial y_c}{\partial x}\right)\right]^2$$

In (4), y_b and y_c are the rotor and casing beam positions which are functions of the degrees of freedom:

$$y_b(x) = f\sin\frac{\pi x}{L} + (e_1 + e_3)\left(\frac{L-x}{L}\right) + (e_2 + e_4)\left(\frac{x}{L}\right)$$
$$y_c(x) = e_3\left(\frac{L-x}{L}\right) + e_4\left(\frac{x}{L}\right) \tag{5}$$

As the HPFTP rotor is strongly held at its ends with bearings, the gyroscopic coupling effects expected from the precession movement of the discs can be neglected, this is the reason for the absence of terms containing the shaft speed ω_s in (4).

Damping can be added to the energy formalism by introducing Rayleigh's dissipation function [5], which, in our case, can be expressed simply as (the contribution of a cross-coupled damping coefficient is neglected)

$$\Re = \frac{1}{2}(c_1\dot{e}_1^2 + c_2\dot{e}_2^2 + c_3\dot{e}_3^2 + c_4\dot{e}_4^2) \tag{6}$$

Defining the Lagrangian as $L = T - V$, we can use (2) and (4) to construct the equations of motion

$$\frac{d}{dt}\frac{\partial L}{\partial \dot{q}_j} - \frac{\partial L}{\partial q_j} + \frac{\partial \Re}{\partial \dot{q}_j} = Q_j \tag{7}$$

The generalized external forces Q_j will be considered as unbalance excitations generated in one or more discs:

$$Q_f = \omega_s^2\sum_{j=1}^5\left[m_jA_j\sin\frac{\pi x_j}{L}\right]\exp(i\omega_s t)$$

$$Q_{e_1} = \omega_s^2\sum_{j=1}^5\left[m_jA_j\frac{L-x_j}{L}\right]\exp(i\omega_s t) \tag{8}$$

$$Q_{e_2} = \omega_s^2\sum_{j=1}^5\left[m_jA_j\frac{x_j}{L}\right]\exp(i\omega_s t)$$

$$Q_{e_3} = Q_{e_4} = 0$$

The amplitude of the complex vector A_j is the amount of eccentricity in each one of the discs, and its phase indicates the location of the center of mass with respect to the disc center.

The result of evaluating (7) is a coupled system of five second order differential equations:

$$M\ddot{\underline{q}} + C\dot{\underline{q}} + K\underline{q} = \underline{Q} \tag{9}$$

Where M, C, and K are the mass, damping and stiffness matrices, which in our case are symmetric. We can find directly the normal vibrational modes (ω_j) of the system by solving the eigenvalue equation

$$\omega_j^2 = [\text{eig}(M^{-1}K)]_j \qquad \text{for} \qquad j = 1\dots5 \tag{10}$$

Data used in this work is shown in tables 1, 2 and 3.

Modulus of Elasticity (E)	1.7162 x10^{11}	N-m^{-2}
Moment of Inertia (I)	29.131 x10^{-7}	m^4
Density (ρ_b)	42.4	kg-m^{-1}
Moment of Inertia (J_b)	$\rho_b L^3/12$	kg-m^2
Length (L)	0.60	m

Table 1. Rotor beam data used in the simplified model

4

	Position (x_j)	Mass (m_j)	Inertia (J_j)
Pump 1st	0.0814	6.257	3.643
Pump 2nd	0.2087	6.257	3.643
Pump 3rd	0.3320	6.098	3.535
Turbine 2nd	0.4739	6.261	3.161
Turbine 1st	0.5386	7.994	3.307
	m	kg	$\times 10^{-2}$ kg-m^{-2}

Table 2. Disc data used in the simplified model - from [7]

Constant	Value (N/m)
k_1	2.1×10^8
k_2	1.5×10^8
k_3	1.9×10^9
k_4	2×10^9

Table 3. Stiffness constants

Table 4 contains the results of applying (10) to compute the normal modes. Results from [7] are also shown. As we can observe there is good agreement for some of the most important modes of the HPFTP.

Frequency (Hz)	Frequency from [7]	Representation
228.8	287.6	Rotor translation + bending
418.2	424.0	Rotor rocking
514.9	513.6	Rotor bending + casing translation
773.6	N.A.	Rotor/casing rocking
1076.7	N.A.	Rotor bending

Table 4. Modal results

To apply the model developed in this section as a signal generator we need to solve (9) in the time domain. This can be done using a standard numerical integrator, and finally identifying the real and imaginary parts of the signal as its components in *y* and *z* respectively.

Fig. 5 shows the results from our model simulating the ignition sequence for the HPFTP. The units have been normalized to g's (9.8 m/s^2) to be expressed in the same way as the output of accelerometers mounted in each one of the positions denoted in Fig. 4. We have assumed a $\beta = 2$ (precise measurements [10] have shown that it is higher than that) to keep the damping constant values relatively low (all four were set to 6000 Ns/m) and avoid instabilities. The cross-coupled force was set between the turbine stages. The time dependent torque and rotor speed profiles were extracted from Rocketdyne's engine balance simulation [12], and for the HPFTP turbines

[10] $H = 2.3$cms and $R = 12.9$cms. The unbalance excitation force was established by displacing the center of mass of the turbine discs by 0.028mm in perpendicular directions.
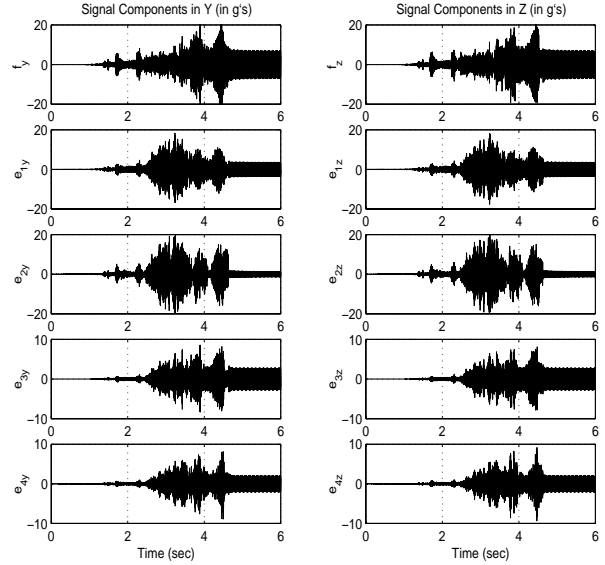

Figure 5. Accelerometer signals - modeled ignition sequence

3. Tracking/Identification Algorithm

As we mentioned in the introduction, tracking and identification of signals is commonly used as a tool in diverse fields, from image processing to satellite communications. Fourier analysis, wavelets and sequential least-squares algorithms are among the methods used for this purpose. In our case, the tracking of the signal is performed using a standard adaptive algorithm (provided by [13] and modified by the first author) that works to minimize the difference between the source signal *s* and its estimate $\hat{s}$. In a discretized form, this difference (called the signal error) is given by

$$\varepsilon_k = \hat{s}_k - s_k \tag{11}$$

where *k* represents the time step. The signal estimate is updated according to

$$\hat{s}_k = \sum_{l=1}^{n-1} \hat{b}_{l(k-1)} w_l + \hat{b}_{n(k-1)} s_{k-n} - s_{k-2n} \tag{12}$$

and the $\hat{b}$ parameters are found after applying the following adaptation law

5

$$\hat{b}_{lk} = \hat{b}_{l(k-1)} - \gamma\varepsilon_k w_l \qquad \text{for} \quad l = 1\ldots(n-1)$$
$$\hat{b}_{nk} = \hat{b}_{n(k-1)} - \gamma\varepsilon_k s_{k-n} \qquad (13)$$

where n is the number of modes to be tracked and identified in the signal, and w_l is given by

$$w_l = s_{k-l} + s_{k+l-2n} \qquad \text{for} \quad l = 1\ldots(n-1) \qquad (14)$$

the gain γ in the adaptation law is updated at each time step with

$$\gamma = \left[1 + s_{k-n}^2 + \sum_{l=1}^{n-1} w_l^2 \right]^{-1} \qquad (15)$$

The origin of (11-15) arises after considering a signal generated by the addition of n sinusoids, each with a defined amplitude and frequency

$$s(t) = A_1 \sin(\omega_1 t) + \ldots + A_n \sin(\omega_n t) \qquad (16)$$

Each one of the components in (16) can be expressed as the solution of a discrete second order difference equation such as

$$s_{k+1} = a s_k - s_{k-1}$$
$$\text{with} \qquad a = 2\cos(\omega t_s) \qquad (17)$$

where t_s is the length of the time step. Using (17) we can discretize and represent (16) as a solution of a $2n^{\text{th}}$ order difference equation, which in terms of its characteristic polynomial can be written as

$$[(v^2 - a_1 v + 1)\ldots(v^2 - a_n v + 1)]s_k = 0$$
$$\text{where} \qquad v^m s_k = s_{k+m} \qquad (18)$$

It can be shown, after expanding and grouping terms, that the negatives of the $\hat{b}$ parameters in (12) are the coefficients of the powers of v in (18). In this way we can recover the values of a after finding the roots of the polynomial constructed by expanding (18). Given t_s we can get the frequencies ω from a directly.

If the error (11) is small enough compared with the magnitude of the signal, then the estimates of b will be close to their real values and therefore, the frequencies comprising the signal can be correctly identified.

It was found that it is important for the identification to work that the sampling frequency ($1/t_s$) be fixed close to the Nyquist limit, i.e., the sampling frequency should be twice the highest frequency present in the sampled signal. If the sampling frequency is increased above this limit, the tracking algorithm will generate estimates of the b parameters which correspond to spurious high frequencies. It is possible that these high frequencies will allow a close estimation of the signal at the sampling points exclusively, forcing the error (11) to be small, but missing completely the identification of frequencies in the observed signal.

4. Tracking/Identification Examples

In this section we will discuss some preliminary results from the tracking algorithm discussed above. The signals analyzed were created with the HPFTP model described in section 2. The idea of using the dynamic model as a signal generator is to explore the behavior of the signal processing algorithm when confronted with data that resembles real signals from the engine. We have identified three cases in which the utility of the algorithm can be tested. In all instances, the signal analyzed was taken from an hypothetical accelerometer sensor mounted near the outside end of the pump bearing (point p in Fig. 3) and aligned in the y direction. This location allows a direct measurement of $\ddot{e}_{3y}$. Measurements of vibrations in the rotor and the inner end of the bearings are extremely difficult because of the constraints in space available, implementation issues and working environment, which can be extremely harsh. On the other hand, we found that position p may be compatible with a series of new accelerometers developed at the C. S. Draper Laboratory [14]. This devices are quite small as they are constructed with the same silicon-based technology of microcircuits, and their specifications appear to be adequate to work with typical signals generated by rocket engine turbomachinery. Since we will deal in these examples with multimodal identification of at least 6 modes, we set the algorithm with $n = 7$ to include all of them, and as the largest modal frequency is close to 1 kHz, we will fix the sample frequency at 2 kHz in agreement with Nyquist.

4.1 Steady state signal at 100% RPL

In this example, the dynamic model was used to generate a steady state signal containing 2 sec of data. The rotor was set at an angular speed of 3580 rad/sec (570 Hz) which is the nominal for 100% RPL (rated power level) operation of the SSME. The generated signal, plus its FFT PSD spectrum are shown in Fig. 6.
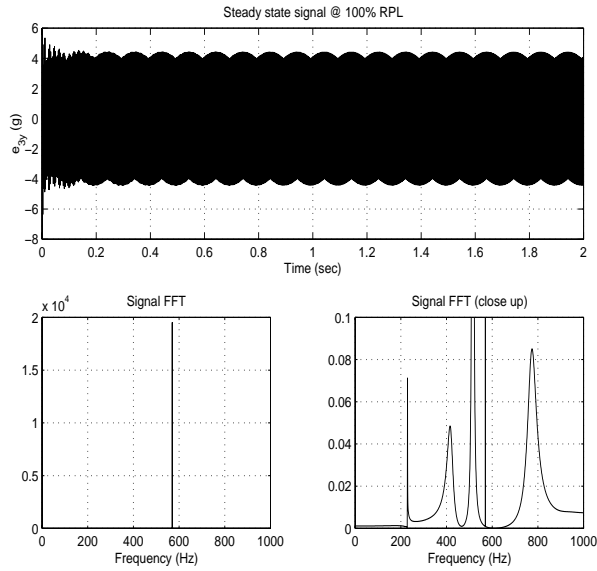
Figure 6. Steady state signal @ 100% RPL

As the turbomachine is operating relatively far away from resonance (the closest natural mode is at 515 Hz), the natural mode components of the signal had been damped out and their magnitudes are very small when compared with the synchronous response. Nevertheless, this signal was introduced to the algorithm and the results are shown below.
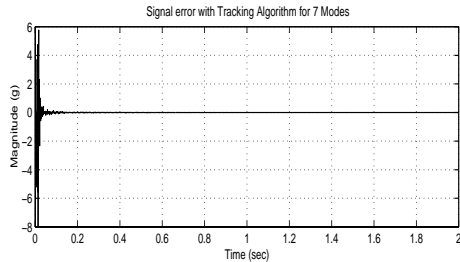

Figure 7. Signal error: steady state @ 100% RPL

Fig. 7 shows how the error (11) approaches zero indicating tracking of the signal. In Fig. 8 we observe how the frequencies are also identified (compare with table 4). This result gives an indication of how sensitive this algorithm can be to small signal components. On the other hand, if we are just interested in tracking the synchronous response, a lower (n) mode order can be used.

The identified frequency close to 925 Hz represents the one at 1076 Hz in table 4. Its misplacement occurs because its value is higher than the Nyquist limit and an error emerged in the discretization procedure. This can be avoided by taking a slightly larger sampling frequency to include frequencies with higher values. More

interesting than this is the fact that the algorithm identified this particular mode while it was invisible in the FFT spectrum, even at the scale presented in the close up view of Fig. 6.
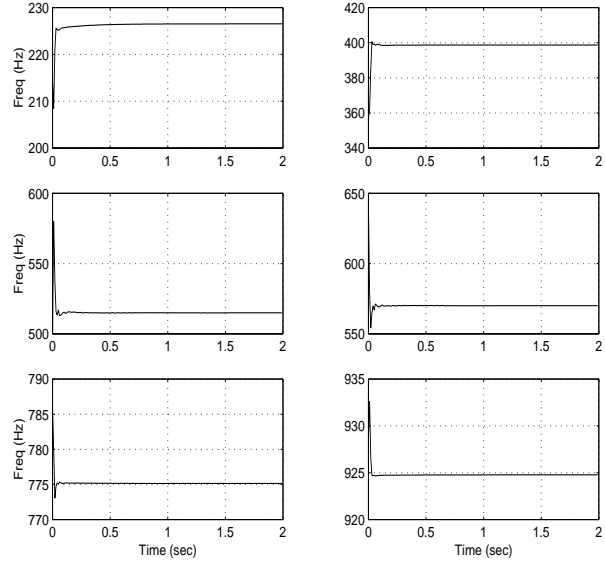

Figure 8. Frequency identification: steady state @ 100% RPL

4.2 Sudden change in RPL from 100% to 109%

In this case, a steady state signal is generated at 100% RPL. At t = 1 sec a sudden change in RPL to 109% happens, increasing the rotor speed to 3800 rad/sec (605 Hz). The signal plus its FFT spectra before and after the change are shown in Fig. 9.
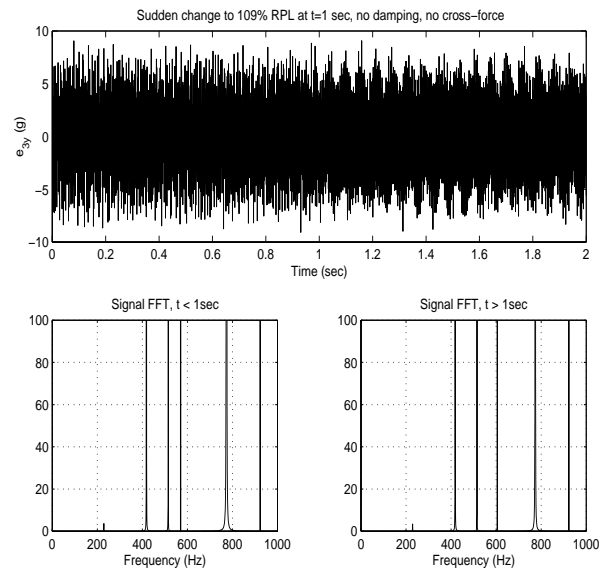

Figure 9. Sudden increase in RPL at t=1 sec

7

In this particular case we have eliminated the damping and the cross-forces by setting β = 0. The reason for this is to avoid the decay of the normal modes and test the ability of the algorithm to adjust to sudden external perturbations, such as the increase in rotor speed. The error signature from the tracking algorithm for this example is shown in Fig. 10.
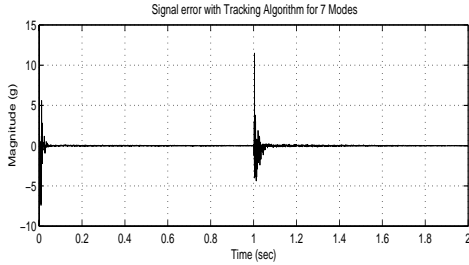

Figure 10. Signal error: change in RPL at t=1 sec

Once more, tracking of the signal was performed and also good identification of all the natural and synchronous modes was obtained as depicted in Fig. 11. The small jump in the modal frequency located at 229 Hz is due to the fact that its amplitude remained very small as compared with the rest of the signal components (as can be seen in the spectra of Fig. 9 where the scale was set to include all the modes: the ratio of the synchronous mode amplitude to this natural mode amplitude is approximately 50.) The jump in the synchronous response frequency from 570 to 605 Hz was sharply identified, while natural frequencies other than the lowest where correctly shown to remain unchanged.
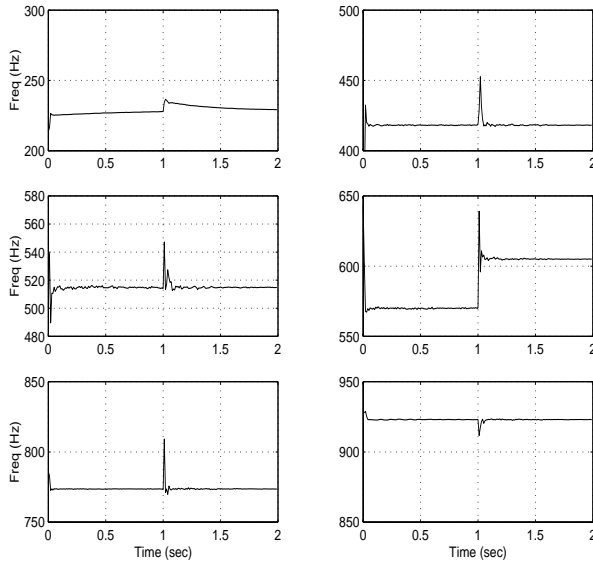

Figure 11. Frequency identification: change in RPL at t=1 sec

4.3 Sudden change in the stiffness matrix

In this case (also without damping and cross-forces), a structural failure is simulated by changing the stiffness constant of bearing #1: k_1 takes a value of 1×10^8 N/m at t = 0.3 sec while the engine operates at 100% RPL. This kind of failure produces the signal and FFT spectra shown in Fig. 12.
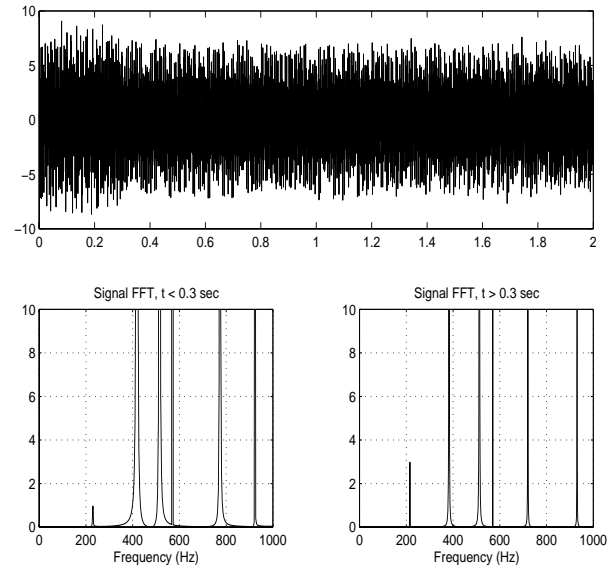

Figure 12. Sudden change of k_1 at t=0.3 sec

Using (10), we can recalculate the natural frequencies for t > 0.3 sec. The results are shown in table 5.

Frequency (Hz)	Representation
215	Rotor translation + bending
383	Rotor rocking
513	Rotor bending + casing translation
720	Rotor/casing rocking
930	Rotor bending

Table 5. Modal results with change in k_1

Fig. 13 shows the error profile obtained after introducing the signal generated into the algorithm.
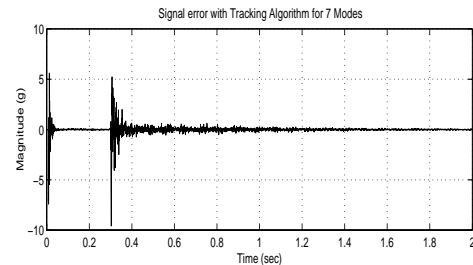

Figure 13. Signal error: change in k_1 at t=0.3 sec

8

The error close to zero indicates positive signal tracking, and identification was also well performed as indicated by the results of Fig. 14.
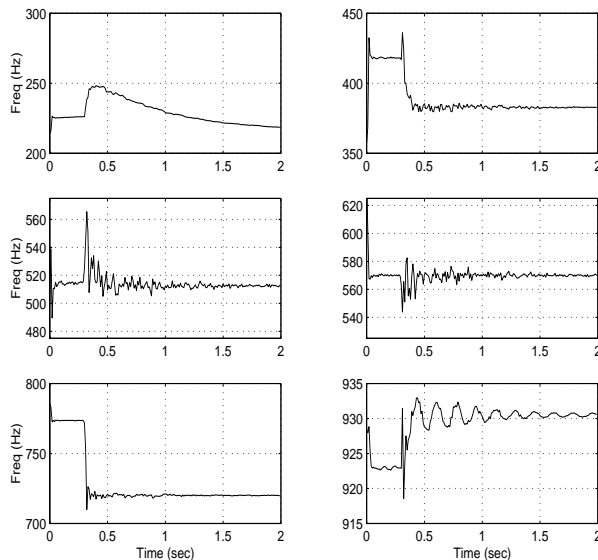

Figure 14. Frequency identification: change in k1 at t=0.3 sec

It is interesting to note that with this particular change in stiffness, the highest frequency dropped below 1 kHz, putting it within the range imposed by Nyquist. In this way, good identification was performed at the correct frequency. It can be also noticed, how the frequency close to 220 Hz was slowly identified; the reason can be attributed once more to its relatively small amplitude as compared with the rest of the modal responses.

4.4 Limitations of the algorithm

Despite the success shown in the preceding examples, several limitations remain to be overcome, and work continues in this direction:

(a) The algorithm performs poorly in periods when conditions change in a continuous fashion, as for example during start-up or power adjustment transients. It is interesting to observe that <u>sudden</u> changes are identified easily (secs. 4.2, 4.3).

(b) For applications in rocket engines, an assessment of the degree of damping of the various modes is as important as identification of their frequency. This is because of the ever-present risk of negative-damping instabilities fed from the extremely large pool of free energy available in the fluids being pumped or handled. Algorithms capable of identi-

fying small positive or negative damping factors are being therefore investigated.

(c) Robustness of the results needs to be improved, including resilience to unexpected modes or noise.

5. Conclusions

Preliminary results have been presented on the path to a unified liquid rocket HM system utilizing both, thermodynamic and vibratory data. An adaptive tracking algorithm was tested against simulated multi-mode accelerometer data, and good results were obtained for steady or suddenly changing conditions. Required extensions were discussed.

6. References

[1] T. Fox, H. Cikanek and T. Evatt, "Development of the System for Anomaly and Failure Detection Program". SAE Paper 952012, Aerotech '95, L.A., California, Sept. 1995.

[2] R. L. Bickford, T.W. Bickmore, C.M. Meyer and J. F. Zalerajsek, AIAA 96-2827, 32nd Joint Propulsion Conf., Lake Buena Vista, FL, July 1996.

[3] C. M. Meyer, W. A. Maul, A. P. Dhawan, "SSME Parameter Estimation and Model Validity Using Radial Basis Function Neural Networks". Advanced Earth-to-Orbit Propulsion Conference, May 1994.

[4] Wu Jianjun, Zh. Yulin and Ch. Qizhi, "A Real-Time Verification System on Fault Diagnosis Methods for Liquid Propellant Rocket Engine". AIAA 96-2831, 32nd Joing Propulsion Conf., Lake Buena Vista, FL, July 1994.

[5] N. T. Ho, P. Lozano, R. Mangoubi and M. Martinez-Sanchez, "Vehicle Health Monitoring for the SSME". AIAA 97-2821 33rd Joint Propulsion Conference, Seattle, WA, July 1997.

[6] J. N. Juang, "Applied System Identification", Prentice-Hall, 1994.

[7] Mueller, G. R., "Finite Element Models of the Space Shuttle Main Engine", NASA TM-78260, January 1980.

[8] Childs, Dara W., "Turbomachinery Rotordynamics: Phenomena, Modeling and Analysis", Wiley-Interscience, New York, 1993.

[9] Rao, J.S., "Rotor Dynamics", Wiley, New York, 1991.

[10] Martinez-Sanchez M., Jaroux B., Song S.J., and Yoo S., "Measurement of Turbine Blade-Tip Rotordynamic Excitation Forces", ASME Journal of Turbomachinery, Vol. 117, No. 3, July 1995, pp. 384-393.

[11] Goldstein, H., "Classical Mechanics", Addison-Wesley Pub. Co., 1980.

[12] Hybrid Systems Analysis Unit and System Dynamics Unit, "Engine Balance and Dynamics Model", Rockwell International Corporation, Rocketdyne Division, report number RL00001, January 1992.

[13] Prof. Anuradha Annaswamy, personal communication.

[14] J. Bernstein and Ch. Trainor, "Versatile Micromechanical Vibration Sensor and Applications", C.S. Draper Lab Report, 1997.